Modeling the monotonic and cyclic behavior of granular materials by an exponential constitutive function

Zhen-Yu YIN[1,*], Ze-Xiang WU[2], Pierre-Yves HICHER[3]

Affiliations:

[1] Joint professor, Key Laboratory of Geotechnical and Underground Engineering of Ministry of Education; Department of Geotechnical Engineering, College of Civil Engineering, Tongji University, Shanghai, China, 200092; Associate Professor, Research Institute of Civil Engineering and Mechanics (GeM), UMR CNRS 6183, Ecole Centrale de Nantes, France; Email: zhenyu.yin@gmail.com; zhenyu.yin@ec-nantes.fr.

[2] PhD student, Research Institute of Civil Engineering and Mechanics (GeM), UMR CNRS 6183, Ecole Centrale de Nantes, France; email: zexiang.wu@ec-nantes.fr.

[3] Emeritus professor, Research Institute of Civil Engineering and Mechanics (GeM), UMR CNRS 6183, Ecole Centrale de Nantes, France; email: pierre-yves.hicher@ec-nantes.fr.

[*] Corresponding author: Dr. Z.-Y. YIN, Tel. +33240371588, Fax. +33240372535,

Abstract: It is still an open problem to develop a model with a uniform theoretical treatment under various loading conditions. This paper aims to formulate such a model for describing both monotonic and cyclic behaviors of granular materials. An exponential function was adopted to reproduce the stress-strain relation. Within the framework of endochronic models, the shear strain component was enriched with an absolute term in order to account for a reverse loading effect during shearing. The capacity of the basic model with four parameters for reproducing the basic features of granular materials was examined. Three numerical schemes for simulating undrained triaxial tests, drained triaxial tests under constant-*p'* or under constant confining stress, under both monotonic and cyclic loadings, were established. Then, three modifications were carried out to enhance the model by introducing a non-linear elasticity, a non-linear stress-dilatancy, and the critical state concept with four additional parameters. The enhanced version of the model showed good performances in simulating triaxial tests on Toyoura sand under various loading conditions: drained, undrained, constant *p'*, constant confining stress, monotonic and

cyclic loadings.

Keywords: granular material, constitutive relations, triaxial tests, cyclic loading, critical state, stress dilatancy.

Introduction

In civil engineering, granular materials can serve as construction fills or foundation soils. Due to their complex behavior, numerous constitutive models have been developed. These models can be classified as: (1) non-linear hypo-elastic models (e.g., Duncan and Chang, 1970), (2) incrementally non-linear models (e.g., Darve and Labanieh, 1982; Darve, 1990), (3) hypo-plastic models (e.g., Wu et al., 1996; Niemunis and Herle, 1997; Masin and Khalili, 2012), (4) elasto-plastic models (e.g., Vermeer 1978; Jefferies, 1993; Yu, 1998; Gajo and Muir Wood, 1999; Taiebat and Dafalias, 2008; Yao et al., 2004, 2008), (5) micromechanics based models (e.g., Chang and Hicher, 2005; Yin et al., 2010, 2014; Chang et al., 2011; Nicot and Darve, 2011, Wan and Pouragha, 2015). In general, the first four categories are phenomenological models which are commonly adopted in engineering practice due to their efficiency in finite element analyses.

According to the mechanical behavior of granular materials, a phenomenological model should be able to describe the frictional behavior (asymptotic relationship between the stress ratio and the shear strain), the contractive or dilative behavior (shear induced volume change), the critical state behavior (the unique ultimate state of a given material attainable in the p'-q and the e-p' planes for any initial state). The phenomenological models which can successfully capture all these mechanical features require usually more than 10 parameters with more or less complicated formulations. Therefore, it is still an open problem to develop a model with simple formulations and a small number of parameters.

This paper attempts to formulate a simple model with few parameters able to model both monotonic and cyclic behaviors of granular materials. The key formulation followed the framework of endochronic models adopting exponential function in which the absolute shear strain was used to account for a reverse loading effect in shearing. A stress dilatancy relation was developed for the shear induced volume change. Then the basic model was examined on reproducing the basic features of granular materials with establishing three triaxial test simulation schemes. After that, a non-linear elasticity, a non-linear stress-dilatancy and the

58 critical state concept were introduced to enhance the model. Finally, the predictive ability of the
59 model was examined by simulating various triaxial tests on Toyoura sand under different loading
60 conditions.

61 A model based on an exponential function

62 Basic function

63 Granular materials exhibit a non-linear frictional behavior with an asymptotic relationship
64 between the stress ratio and the shear strain, which is a key point in phenomenological
65 constitutive modeling (Duncan and Chang, 1970; Vermeer, 1978; Jefferies, 1993; Biarez and
66 Hicher, 1994). This frictional asymptotic response can be described by various mathematical
67 functions, for example, the hyperbolic or exponential functions (see Figs. 1(a)-(b) for given
68 values of *a* and *b*),

69 $$\eta = \frac{b\gamma}{1/a + \gamma} \quad \text{or} \quad \eta = b\left(1 - \mathrm{e}^{-a\gamma}\right) \tag{1}$$

70 In non-linear constitutive modeling, the incremental form has to be considered and the above
71 functions can be rewritten in an incremental form:

72 $$\dot{\eta} = \frac{ab\dot{\gamma}}{\left(1 + a\gamma\right)^2} \quad \text{or} \quad \dot{\eta} = ab\dot{\gamma}\left(1 - \frac{\eta}{b}\right) \tag{2}$$

73 However, the Eq.(1) or (2) is not able to describe the reversed asymptotic relationship
74 between the stress ratio and the shear strain during unloading. In order to model the cyclic
75 behavior of granular materials, the above equations should be extended to unloading and
76 reloading conditions.

77 As suggested by Sindler (1978) for an endochronic model, the incremental form of the
78 exponential function can be enriched by taking into account the absolute value of the shear strain
79 increment:

80 $$\dot{\eta} = ab\left(\dot{\gamma} - \frac{\eta}{b}|\dot{\gamma}|\right) \tag{3}$$

81 Then for the unloading, the shear strain increment changes its sign from positive to negative

which mathematically results in an unloading asymptotic curve with a twice initial stiffness of loading stage (see Fig. 1(c) for given values of *a* and *b*). Thus, this formulation extends the function from loading to reverse loading, and thus makes this function applicable to describe the cyclic behavior. Therefore, Eq.(3) has been adopted as a basis for the development of the model, as presented in the following sections.

Basic model under triaxial condition

Under triaxial condition, the stress ratio $\eta = q/p'$ is defined by the deviatoric stress q ($q = \sigma_a - \sigma_r$) and the mean effective stress p' ($p' = (\sigma'_a + 2\sigma'_r)/3$) with σ_a and σ_r the axial and radial stresses, respectively. Eq.(3) can be re-written in the following form:

$$\dot{\eta} = G_\eta \left[\dot{\varepsilon}_d - \left(\frac{\eta}{M_p} \right) |\dot{\varepsilon}_d| \right] \tag{4}$$

where $\dot{\varepsilon}_d = 2\left(\dot{\varepsilon}_a - \dot{\varepsilon}_r\right)/3$ is the deviatoric strain increment function of the axial and radial strain increments, M_p is the strength ratio, and G_η is the initial stiffness.

The stress ratio increment can be derived as:

$$\eta = \frac{q}{p'} \Rightarrow \dot{\eta} = \frac{\dot{q}}{p'} - \frac{q}{p'^2}\dot{p}' = \left(\dot{q} - \eta \dot{p}'\right)\frac{1}{p'} \tag{5}$$

Combining Eq.(5) and Eq.(4), we obtain:

$$\dot{q} = G_\eta \left[p'\dot{\varepsilon}_d - \left(\frac{q}{M_p} \right) |\dot{\varepsilon}_d| \right] + \frac{q}{p'}\dot{p}' \tag{6}$$

According to this equation, the initial slope of the curve q-ε_d, termed as three times the shear modulus G, can be obtained by assuming that q is very small for a small value of ε_d:

$$3G = \frac{\partial q}{\partial \varepsilon_d} = G_\eta \left(p' - \frac{q}{M_p} \right) \doteq G_\eta p' \Rightarrow G_\eta = \frac{3G}{p'} \tag{7}$$

Substituting Eq.(7) into Eq.(6), we obtain

$$\dot{q} = 3G \left[\dot{\varepsilon}_d - \left(\frac{q}{p'M_p} \right) |\dot{\varepsilon}_d| \right] + \frac{q}{p'}\dot{p}' \tag{8}$$

A volumetric strain is usually induced during shearing, known as stress-dilatancy behavior. The stress-dilatancy relationship suggested by Roscoe *et al*. (1963) has been modified in order to satisfy both loading and unloading conditions:

$$\frac{\dot{\varepsilon}_v^{in}}{\dot{\varepsilon}_d} = M_{pt} - \frac{q}{p'} \Rightarrow \frac{\dot{\varepsilon}_v^{in}}{\dot{\varepsilon}_d} = \frac{\dot{\varepsilon}_d}{\left|\dot{\varepsilon}_d\right|} M_{pt} - \frac{q}{p'} \tag{9}$$

where $\dot{\varepsilon}_v^{in}$ is the shear strain induced volumetric strain increment. In Eq.(9) $\dot{\varepsilon}_d > 0$ during loading results in $\dot{\varepsilon}_d / \left|\dot{\varepsilon}_d\right| = 1$ and a linear relationship between $\dot{\varepsilon}_v^{in} / \dot{\varepsilon}_d$ and q/p' with an intersection value of M_{pt} at $q/p' = 0$ (see Fig. 2(a)); and $\dot{\varepsilon}_d < 0$ during unloading results in $\dot{\varepsilon}_d / \left|\dot{\varepsilon}_d\right| = -1$ and a linear relationship between $\dot{\varepsilon}_v^{in} / \dot{\varepsilon}_d$ and q/p' with an intersection value of -M_{pt} at $q/p' = 0$ (see Fig. 2(a)), which captured the experimental phenomenon of stress-dilatancy during cyclic loadings (Pradhan, 1989). For a neutral loading with $\dot{\varepsilon}_d = 0$, $\dot{\varepsilon}_d / \left|\dot{\varepsilon}_d\right| = 1$ can be imposed in order to keep the original form of the equation. Note that the proposed model is under the framework of endochronic models using directly the sign of shear strain increment to judge loading or unloading, which is different from general plasticity. The phase transformation stress ratio M_{pt} has been defined in relation to the dilatancy angle of the granular material. Eq.(9) could be simplified as:

$$\dot{\varepsilon}_v^{in} = \frac{\left(\dot{\varepsilon}_d\right)^2}{\left|\dot{\varepsilon}_d\right|} M_{pt} - \frac{q}{p'} \dot{\varepsilon}_d = M_{pt} \left|\dot{\varepsilon}_d\right| - \frac{q}{p'} \dot{\varepsilon}_d \tag{10}$$

The mean effective stress increment can be computed as:

$$\dot{p}' = K\left(\dot{\varepsilon}_v - \dot{\varepsilon}_v^{in}\right) = K\left(\dot{\varepsilon}_v - M_{pt}\left|\dot{\varepsilon}_d\right| + \frac{q}{p'}\dot{\varepsilon}_d\right) \tag{11}$$

where K is the bulk modulus, and $\dot{\varepsilon}_v$ is the volumetric strain increment. Under axisymmetric condition, $\dot{\varepsilon}_v$ is function of the axial and radial strain increments: $\dot{\varepsilon}_v = \dot{\varepsilon}_a + 2\dot{\varepsilon}_r$.

Finally, the basic model is completely defined by Eqs.(8) and (11). Note that the constitutive equations are non-symmetric, and the degree of non-symmetry sharply changes upon strain reversal.

Summary of the basic model parameters

The basic model includes four parameters directly related to those present in the Mohr-Coulomb model (see Fig. 2(b)), summarized as follows:

(1) The bulk modulus K and the shear modulus G, which is equivalent to the use of the Young's modulus E and Poisson's ratio υ ($E = 9KG/(3K+G)$, $\upsilon = (3K-2G)/(6K+2G)$) as in the Mohr-Coulomb model, or the use of G and υ measured from drained triaxial tests. Since the small strain stiffness was not considered in this model, the elastic parameters can be calibrated directly from conventional tests instead of specified small strain tests.

(2) The strength ratio M_{p} depends on the friction angle of the material, as in the Mohr-Coulomb model: $M_p = 6\sin\phi_c/(3-\sin\phi_c)$.

(3) The phase transformation stress ratio M_{pt} depends on the dilation angle ψ as in the Mohr-Coulomb model: $M_{pt} = M_p - 2\sin\psi/(1-\sin\psi)$.

Note that a cohesion can also be easily introduced in the model if p' in Eqs.(8) and (11) is replaced by $p'+2c/M_{\mathrm{p}}$, with c the cohesion as in the Mohr-Coulomb model.

Simulation schemes and predictive performance of the basic model

In this section, three simulation schemes for undrained triaxial tests, drained triaxial tests under constant-p' and under constant confining stress, for both monotonic and cyclic loadings have been established. Then, for a given set of parameters, the predictive performance of the basic model was examined according to the results of experimental investigations.

Undrained triaxial test simulations

Eqs.(8) and (11) can be used directly for simulating the tests under full strain control. For example, $\dot{\varepsilon}_d = 0$ is imposed for isotropic compression implied by Eqs.(8) and (11); $\dot{\varepsilon}_v = 0$ is imposed for undrained shearing. The undrained triaxial test was simulated by a given set of parameters, as shown in Figures 3(a)-(b). Different values of the phase transformation stress ratio led to different typical behaviors of the granular material, depending on its initial density.

To simulate the undrained cyclic triaxial test under stress control with given values of the maximum and minimum deviatoric stresses, a deviatoric strain increment was first imposed with

null volumetric strain increment. The deviatoric strain reversal was then conducted when the current deviatoric stress exceeded the maximum or minimum deviatoric stress. In other word, this stress control test was numerically conducted under strain control. With this technique, an undrained cyclic triaxial test was simulated by a given set of parameters, as shown in Figures 3(c)-(d). Again, different values of the phase transformation stress ratio led to different typical behaviors of the granular material, i.e., cyclic mobility for dense sand and cyclic liquefaction for loose sand.

Drained constant-p' test simulations

Under the drained constant-*p'* test condition, the incremental mean effective stress is null. Thus, the volumetric strain and the deviatoric stress can be obtained from Eqs.(8) and (11):

$$\dot{p}' = 0 \Rightarrow \begin{cases} \dot{\varepsilon}_v = M_{pt}\left|\dot{\varepsilon}_d\right| - \dfrac{q}{p'}\dot{\varepsilon}_d \\ \dot{q} = 3G\left[\dot{\varepsilon}_d - \left(\dfrac{q}{p'M_p}\right)\left|\dot{\varepsilon}_d\right|\right] \end{cases} \tag{12}$$

A drained constant-*p'* test can, therefore, be simulated by imposing the incremental deviatoric strain in Eq.(12).

Tests under monotonic loading were first simulated by a given set of parameters, as shown in Figures 4(a)-(b). Different values of the phase transformation stress ratio gave different typical contractive and dilative behaviors of the granular material, corresponding to dense or loose sand. However, the calculated deviatoric stress appeared independent of the stress dilatancy, as it is the case for many simple models, such as the Mohr-Coulomb model, the Duncan-Chang model (Duncan and Chang, 1970), the basic hypoplastic model of Wu and Kolymbas (1996), the hardening soil model of Schanz et al. (1999), etc.. This aspect needs, therefore, to be improved.

The simulation technique for a cyclic test under stress control with given values of the maximum and minimum deviatoric stresses is similar to the one used for an undrained test, as presented in the previous section. Another cyclic test under strain control condition was simulated by imposing directly the strain increment between the maximum and minimum imposed strain values. The deviatoric strain control cyclic test was simulated with a given set of parameters, as shown in Figures 4(c)-(d). Again, different values of the phase transformation

stress ratio gave different typical behaviors of the granular material, i.e., a progressive dilation for a dense sand and a progressive contraction for a loose sand. Similar to the results obtained for a monotonic test, the deviatoric stress-strain response appeared independent of the stress-dilatancy, which needs also to be improved.

Conventional drained triaxial test simulations

In a conventional drained triaxial test, the confining stress is maintained constant. Thus, the ratio between the incremental deviatoric stress and the incremental mean effective stress is equal to 3. From Eqs.(8) and (11), the volumetric strain and the deviatoric stress can be obtained as follows:

$$\dot{q} = 3G\left[\dot{\varepsilon}_d - \left(\frac{q}{p'M_p}\right)\left|\dot{\varepsilon}_d\right|\right] + \frac{q}{p'}\dot{p}' \xrightarrow{\dot{q}=3\dot{p}'} \dot{q} = 3G\left[\dot{\varepsilon}_d - \left(\frac{q}{p'M_p}\right)\left|\dot{\varepsilon}_d\right|\right] \Big/ \left(1 - \frac{q}{3p'}\right) \tag{13}$$

$$\dot{p}' = \frac{\dot{q}}{3} \tag{14}$$

$$\dot{\varepsilon}_v = \frac{\dot{p}'}{K} + M_{pt}\left|\dot{\varepsilon}_d\right| - \frac{q}{p'}\dot{\varepsilon}_d \tag{15}$$

Then, the conventional drained triaxial test can be simulated by imposing an incremental deviatoric strain, following the order of the equations (13) to (15).

As for the constant-*p'* tests, monotonic and cyclic loadings were simulated, based on a given set of parameters, as shown in Figure 5. The same conclusions as for the constant-*p'* test could be made, except for the cyclic test which presented a less symmetric behavior between the unloading and reloading phases.

Enhancement of the model

Non-linear elasticity

To introduce the dependency of the elastic stiffness on the density and the mean effective stress, the expression of the hypo-elastic shear modulus *G* suggested by Richart et al. (1970) has been adopted:

202 $$G = G_0 \frac{(2.97-e)^2}{(1+e)} \left(\frac{p'}{p_{at}} \right)^n, \; K = K_0 \frac{(2.97-e)^2}{(1+e)} \left(\frac{p'}{p_{at}} \right)^n \tag{16}$$

203 with two parameters K_0 & G_0 instead of K & G, and one additional parameter n (typically 0.5-
204 0.7). The atmospheric pressure p_{at} = 101.325 kPa was chosen as the reference stress.

205 To identify the change due to the consideration of a non-linear elasticity, monotonic
206 constant-p' tests were simulated with a given set of parameters and three different initial void
207 ratios, as shown in Figure 6. The results demonstrated that an increase in the void ratio led to a
208 smaller initial slope of the stress-strain curve and a less dilative behavior, in agreement with the
209 general experimental phenomena.

210 **Critical state concept**

211 Several formulae for expressing the critical state concept have been proposed. The most
212 typical one is the linear formula in the e-logp' plane. The relationship has traditionally been
213 written as follows:

214 $$e_c = e_{ref} - \lambda \ln \left(\frac{p'}{p_{ref}} \right) \tag{17}$$

215 where e_{ref} is a reference void ratio corresponding to a reference mean effective stress p_{ref}; λ is the
216 slope of the critical state line (CSL) in the e-log p' plane. Therefore, two parameters (e_{ref} and λ)
217 are required for the definition of the CSL. The advantage of this formula is the simplicity of its
218 form. However, experimental results have shown that the CSL is not always linear in the e-log p'
219 plane, and, mathematically, the critical void ratio e_c could become negative for high stress levels,
220 which is physically incorrect. Note that the very high stress level still exists in geotechnical
221 structures, like pile tip during its installation.

222 More recently, another formula has been proposed by Li and Wang (1998) who assumed a
223 non-linear critical state line in the e-logp' plane, representing an extension of the linear formula
224 with one additional parameter ξ:

225 $$e_c = e_{c0} - \lambda \left(\frac{p'}{p_{at}} \right)^{\xi} \tag{18}$$

226 where the additional parameter ξ controls the non-linearity of the critical state line, giving a more

flexible and accurate description according to experimental data, especially for very low to moderate stress levels. However, for high stress levels the positiveness of critical void ratio e_c could not be guaranteed, and possibly cause numerical problem of some local elements in finite element modeling. To overcome this difficulty, Gudehus (1997) suggested a third formula of the CSL, which is also a non-linear formula but with a "s" form by considering an ultimate critical void ratio at very high stress levels. It can be expressed as follows:

$$e_c = e_{cu} + \left(e_{c0} - e_{cu}\right)\exp\left(-\left(\frac{p'}{p_{at}\cdot\lambda}\right)^{\xi}\right) \tag{19}$$

where e_{cu} is the critical void ratio when $p'\to\infty$. This expression eliminates the possibility of a negative value of the critical void ratio at high stress levels. However, two more parameters have to be determined.

Considering the advantage of the second formula, we adopted the expression of Eq.(18). The problem of a possible negative void ratio is due to the fact that the formula is based on a semi-logarithmic plot. If a double-logarithmic plot is used, then Eq.(18) can be revised as:

$$\log\left(e_c\right) = \log\left(e_{c0}\right) - \lambda\left(\frac{p'}{p_{at}}\right)^{\xi} \tag{20}$$

which can be rewritten as,

$$e_c = e_{c0}\exp\left[-\lambda\left(\frac{p'}{p_{at}}\right)^{\xi}\right] \tag{21}$$

Given different values of the parameters e_{c0}, λ, ξ, different curves can be obtained by Eq.(21), as shown in Figure 7. It can be concluded that ξ controls the slope of the CSL after the inflection point (Fig. 7(a)), λ controls the position of the inflection point (Fig. 7(b)), and the combination of the three parameters gives access to an almost constant slope of the CSL as in Eq.(17) (Fig. 7(c)). This enhanced formula gives the advantage of a non-linear CSL, and at the same time imposes the positiveness of the void ratio with three parameters as input.

With the critical state concept, the density state of the soil can be defined by the ratio e_c/e or the distance e_c-e, where e is the current void ratio and e_c is the critical void ratio at the current

stress state *p'*, obtained from the equation of the CSL. This implies: $e_c/e < 1$ or $e_c\text{-}e < 0$ for loose packing, $e_c/e > 1$ or $e_c\text{-}e > 0$ for dense packing, and $e_c/e = 1$ or $e_c\text{-}e = 0$ when the initial state lies on the CSL in the *e-p'* plane. In agreement with experimental results obtained by Biarez and Hicher (1994), the density state effect to the stress-strain-strength behavior was implemented into the model by the following relation:

$$\phi_p = \arctan\left(\frac{e_c}{e}\tan\phi_c\right), \quad \phi_{pt} = \arctan\left(\frac{e}{e_c}\tan\phi_c\right) \tag{22}$$

The expression of the mobilized peak friction angle ϕ_p in Eq.(22) shows that, in a loose structure, ϕ_p is initially smaller than the critical friction angle ϕ_c. On the other hand, a dense structure provides a higher degree of interlocking. Thus, ϕ_p is greater than ϕ_c. When the loading stress reaches the peak stress, a dense structure will dilate and the degree of interlocking will decrease. As a consequence, the peak friction angle will be reduced, which results in a strain-softening phenomenon.

The mobilized phase transformation angle ϕ_{pt} in Eq.(22) implies that in a loose structure with $e>e_c$, ϕ_{pt} is bigger than ϕ_c, which leads to a continuously contractive behavior; in a dense structure with $e<e_c$, ϕ_{pt} is smaller than ϕ_c, which imposes to a dense structure to be initially contractive, and then dilative during a deviatoric loading.

For both loose and dense structures, when the stress state reaches the critical state line, the void ratio e becomes equal to the critical void ratio e_c, and no volume change will take place any longer. Thus, the constitutive equations guarantee that stress and void ratio reach simultaneously the critical state in the *p'-q-e* space. Note that Eq.(22) gives a similar density effect as in the model suggested by Manzari and Dafalias (1997), but in a different form.

Using the above mobilized peak friction angle ϕ_p and the mobilized phase transformation angle ϕ_{pt}, and accounting for the Lode angle dependency, we can express the peak strength ratio M_p and the phase transformation stress ratio M_{pt} by the following relations:

$$M_p = \begin{cases} \dfrac{6\sin\phi_p}{3-\sin\phi_p} & \text{in compression} \\ \dfrac{6\sin\phi_p}{3+\sin\phi_p} & \text{in extension} \end{cases}, \quad M_{pt} = \begin{cases} \dfrac{6\sin\phi_{pt}}{3-\sin\phi_{pt}} & \text{in compression} \\ \dfrac{6\sin\phi_{pt}}{3+\sin\phi_{pt}} & \text{in extension} \end{cases} \tag{23}$$

To enhance the model, Eqs.(21)-(23) were introduced in the model presented in the previous section, and then used to simulate conventional drained and undrained triaxial tests on samples with different initial void ratios. As shown in Figure 8, the enhanced model with the critical state concept can well reproduce the density effect on the mechanical behavior of granular materials.

Note that the Eq.(23) can also be applied to the basic model to enhance the strength in extension following the strength criterion of Coulomb or Matsuoka-Nakai (1974) without additional parameters.

Non-linear stress-dilatancy

Experimental investigations showed that the stress path in the *p'-q* plane developed vertically at the beginning of an undrained triaxial loading, which implied that only a very slight volumetric strain was induced at the beginning of the shearing. The stress-dilatancy equation (Eq.(9)) should, therefore, be modified as follows:

$$\frac{\dot{\varepsilon}_v^{in}}{\dot{\varepsilon}_d}=\left(\frac{\dot{\varepsilon}_d}{|\dot{\varepsilon}_d|}M_{pt}-\frac{q}{p}\right)\left[1-\exp\left(-d\left|\eta-\eta^R\right|\right)\right] \tag{24}$$

where η^R is the stress ratio at the strain reversal state, and d is a material constant controlling the non-linearity of the stress-dilatancy. The occurrence of a strain reversal is controlled by the condition "$d\gamma^{(i-1)}*d\gamma^{(i)} < 0$", with $\eta^R = \eta^{(i-1)}$ (*i* represents the current step, and *i-1* the previous step). This non-linear function was introduced into Eq.(11) as follows:

$$\dot{p}'=K\left(\dot{\varepsilon}_v-\dot{\varepsilon}_v^{in}\right)=K\left\{\dot{\varepsilon}_v-\left(M_{pt}\left|\dot{\varepsilon}_d\right|-\frac{q}{p'}\dot{\varepsilon}_d\right)\left[1-\exp\left(-d\left|\eta-\eta^R\right|\right)\right]\right\} \tag{25}$$

The enhanced model was then used to simulate undrained triaxial tests on samples with different initial void ratios. As shown in Figure 9, the introduction of the non-linear stress-dilatancy could improve the quality of the numerical simulations in terms of stress path and deviatoric stress-strain response during undrained loading.

Model validation by experimental data

Different triaxial tests under both monotonic and cyclic loadings on Toyoura sand were selected for validating the model. Toyoura sand is a uniform fine quartzic sand that consists of sub-rounded to sub-angular grains. It has been widely tested (Miura and Yamanouchi, 1975;

Miura et al., 1984; Pradhan, 1989; Verdugo and Ishihara, 1996; Yoshimine et al., 1998; Uchida and Stedman, 2001). Toyoura sand has a maximum void ratio of 0.977, a minimum void ratio of 0.597, and a specific gravity of 2.65.

Three undrained triaxial tests performed by Verdugo and Ishihara (1996) under a confining stress of 1000 kPa with different initial void ratios was used to calibrate the model parameters. The three parameters defining the critical state line were measured from the position of the critical states in the e–log p' plane (see Fig. 10(a)). Common values of the elastic parameters υ = 0.3 and n = 0.67 were adopted. The critical friction angle was measured from the stress paths in the p'-q plane (see Fig. 10(b)). The shear stiffness parameter G_0 and the stress-dilatancy parameter d were obtained by curve fitting of three undrained tests (Figs. 10(b)-(c)). The values of all the parameters are summarized in Table 1.

Triaxial tests under monotonic loading

Verdugo and Ishihara (1996) conducted a series of monotonic drained and undrained triaxial tests on isotropically consolidated samples of Toyoura sand with a mean diameter D_{50} = 0.17 mm and a uniformity coefficient C_u = 1.7: (1) drained triaxial tests with void ratios ranging from 0.810 to 0.996 under constant lateral stress of 100 kPa and 500 kPa, and (2) undrained triaxial tests with void ratios ranging from 0.735 to 0.907 under different confining pressures from 0.1 MPa to 3 MPa. The above calibrated parameters were used to predict all these tests.

Figure 11 shows the comparison between experimental data and numerical results for drained triaxial compression tests on isotropically consolidated samples. Figure 12 shows the comparison between experimental data and numerical results for the undrained triaxial compression tests on isotropically consolidated samples of the same Toyoura sand. The tests covered an extensive range of confining pressures and void ratios. Very loose, loose, and medium sand were tested in conventional triaxial drained and undrained testing. The comparison between the test results and the model predictions shows an overall good agreement. Note that for drained tests on very loose sand the stiffness at small strains are over-predicted, which can be further improved by considering the feature of small strain stiffness.

Drained cyclic triaxial tests

Pradhan (1989) conducted drained cyclic triaxial tests on Toyoura sand. However, the sand

used by Pradhan (1989) came from a batch different from the one used by Verdugo and Ishihara (1996). Thus, the index properties were slightly different. The same values of the parameters determined from the tests of Verdugo and Ishihara (1996) were used to simulate the drained cyclic test, except for the value of ϕ_c = 32.3° in compression according to the drained test with loading-unloading and reloading.

Figures 13(a)-(c) show the comparison between experiments and predictions for the drained cyclic triaxial test on loose Toyoura sand with an initial void ratio e_0 = 0.845 under constant p' = 98 kPa. Figures 13(d)-(f) show the comparisons for a dense Toyoura sand with an initial void ratio e_0 = 0.653 under constant p' = 98 kPa. Figure 14 shows the comparisons between experiments and predictions for the drained cyclic triaxial test on loose Toyoura sand with an initial void ratio e_0 = 0.863 under constant confining stress p'_0 = 98 kPa. A good agreement was achieved between experimental data and numerical simulations. The slight difference in the volumetric strain might be due to sample differences since the values of the parameters used for predicting this test were determined from a different test. The enhanced model captured the overall trend: at small strain amplitudes, loose sand densifies and dense sand dilates.

Undrained cyclic triaxial tests

Uchida and Stedman (2001) conducted undrained cyclic triaxial tests on Toyoura sand. In each test, an axial strain of 1% magnitude was applied in each cycle until the liquefaction was obtained. The samples were prepared at two relative densities of 30% and 50% and subjected to two initial confining pressures of 200 kPa and 400 kPa. The experimental and numerical results for the two samples are shown in Figure 15. The model parameters calibrated from the monotonic tests were used for the predictions of the cyclic tests. The model reproduces the general trend as depicted by the test. Despite the difference in the evolution of the mean effective stress between experiments and simulations, which may be attributed to the slight difference in properties (like anisotropy) among sands from different batches and the lack of considering the internal fabric effect, the fact that a looser Toyoura sand had a greater liquefaction potential under higher confining pressure was well determined by the model.

Simulations of undrained cyclic tests at constant stress amplitude with q_{max} = 55 kPa and q_{min} = -55 kPa (noted as q_{cyc} = 55 kPa for symmetric loading condition) were conducted on samples with different initial void ratios by using the above values of the model parameters. As expected,

the dense sample exhibited a cyclic mobility phenomenon (Figs. 16(a)-(b)), the medium dense sample exhibited also a cyclic mobility with higher deformations and reached an almost liquefied state in a fewer number of cycles than the dense sample (Figs. 16(c)-(d)). The loose sample reached a complete liquefaction with large deformations in a few number of cycles (Figs. 16(e)-(f)). Thus, the proposed model was able to predict the dependence of the liquefaction potential on the relative density of the sand.

Furthermore, for a given density (e_0 = 0.865) and above set of parameters, simulations of undrained cyclic tests under different conditions were carried out with: stress ratios (q_{cyc}/p'_0 = 0.12, 0.24, 0.36) shown in Figures 17(a)-(b), and with different types of cycles in terms of non-symmetric loading condition (at cyclic deviatoric stress q_{cyc} = 60 kPa with different static deviatoric stresses q_s = 0, 30, 80 kPa) shown in Figures 17(c)-(d). Again, the model can capture the experimental trends (e.g. Yang and Sze, 2011) for the effects of stress ratio and symmetric/ non-symmetric loading condition during undrained cyclic loadings.

Note that for simulating more precisely undrained cyclic tests, the model still needs further enhancement, such as the intergranular strain effect suggested by Niemunis and Herle (1997).

Conclusion

A non-linear incremental model based on a simple exponential function was first suggested. Three simulation schemes for modeling undrained triaxial tests, drained triaxial tests under constant-*p'* and under constant confining stress, and cyclic tests under stress control were established. With only four parameters, the model formulated in axisymmetric condition demonstrated a good performance in reproducing basic features of a granular material under both monotonic and cyclic loading conditions.

Then, a non-linear elasticity, a non-linear stress-dilatancy, and the critical state concept were introduced gradually to enhance the model. The capacity of the enhanced model with eight parameters was evaluated by simulating various triaxial tests on Toyoura sand under different conditions, i.e., undrained tests, drained constant *p'* tests, drained constant confining stress tests, monotonic and cyclic loadings. Overall, a good performance was achieved over all the simulations.

Future work will focus on the extension of the model in the general stress space for solving

boundary value problems, in which the physical consideration of fabric anisotropy (e.g. Li and Dafalias, 2012; Gao et al., 2014; Dafalias and Taiebat, 2014) should be incorporated.

Acknowledgment

This study was substantially supported by the Natural Science Foundation of China (No. 51579179), and the Region Pays de la Loire of France (project RI-ADAPTCLIM).

References

Biarez, J., and Hicher, P.-Y. (1994). Elementary mechanics of soil behaviour: saturated remoulded soils, AA Balkema, France

Chang, C.S. and Hicher, P.Y., 2005. "An elasto-plastic model for granular materials with microstructural consideration". *International Journal of Solids and Structures*, 42(14), 4258-4277.

Chang, C., Yin, Z.-Y., and Hicher, P.-Y. (2010). "Micromechanical analysis for interparticle and assembly instability of sand." *Journal of Engineering Mechanics*, 137(3), 155-168.

Dafalias, Y.F., and Taiebat, M. (2014). "Rotational hardening with and without anisotropic fabric at critical state", *Geotechnique*, 64(6): 507-511.

Darve, F. (1990). "Incrementally non-linear constitutive relationships." *Elsevier Applied Science*, 213-238.

Darve, F., and Labanieh, S. (1982). "Incremental constitutive law for sands and clays: simulations of monotonic and cyclic tests." *International Journal for Numerical and Analytical Methods in Geomechanics*, 6(2), 243-275.

Duncan J.M., Chang C.-Y. (1970). "Nonlinear analysis of stress and strain in soils." *Journal of the Soil Mechanics and Foundations Division*, 96(5), 1629-1653.

Gajo, A., and Wood, M. (1999). "Severn–Trent sand: a kinematic-hardening constitutive model: the q–p formulation." *Géotechnique*, 49(5), 595-614.

Gao, Z., Zhao, J., Li, X.S., and Dafalias, Y.F. (2014). "A Critical State Sand Plasticity Model Accounting for Fabric Evolution", *International Journal for Numerical and Analytical Methods in Geomechanics*, 38(4): 370-390.

Gudehus, G. (1997). "Attractors, percolation thresholds and phase limits of granular soils." *Proc. Powder and Grains*, 97.

Jefferies, M. (1993). "Nor-Sand: a simple critical state model for sand." *Geotechnique*, 43(1), 91-103.

Li, X. S., and Dafalias, Y. F. (2012). "Anisotropic Critical State Theory: Role of Fabric", *J. Eng. Mechanics, ASCE*, 138(3): 263-275.

Li, X.-S., and Wang, Y. (1998). "Linear representation of steady-state line for sand." *Journal of Geotechnical and Geoenvironmental Engineering*, 124(12), 1215-1217.

Manzari, M. T., and Dafalias, Y. F. (1997). "A critical state two-surface plasticity model for sands." *Geotechnique*, 47(2), 255-272.

425 Mašín, D., and Khalili, N. (2012). "A thermo- mechanical model for variably saturated soils based on
426 hypoplasticity." *International journal for numerical and analytical methods in geomechanics*, 36(12),
427 1461-1485.

428 Matsuoka, H., and Nakai, T. (1974). "Stress-deformation and strength characteristics of soil under three
429 different principal stresses." *Proceedings of JSCE*, 232, pp59–70.

430 Miura, N., Murata, H., and Yasufuku, N. (1984). "Stress-strain characteristics of sand in a particle-
431 crushing region." *Soils and Foundations*, 24(1), 77-89.

432 Miura, N., and Yamanouchi, T. (1975). "Effect of water on the behavior of a quartz-rich sand under high
433 stresses." *Soils and Foundations*, 15(4), 23-34.

434 Nicot, F., and Darve, F. (2011). "The H-microdirectional model: accounting for a mesoscopic scale."
435 *Mechanics of Materials*, 43(12), 918-929.

436 Niemunis, A., and Herle, I. (1997). "Hypoplastic model for cohesionless soils with elastic strain range."
437 *Mechanics of Cohesive-frictional Materials*, 2(4), 279-299.

438 Paradhan, T. B. S. (1990). "The behavior of sand subjected to monotonic and cyclic loadings." [*PhD*
439 *thesis*]. Japan: Kyoto University.

440 Schanz, T., Vermeer, P.A., and Bonnier P.G. (1999). "The hardening soil model: formulation and
441 verification." Beyond 2000 in computational geotechnics, pp 281-296.

442 Taiebat, M., and Dafalias, Y. F. (2008). "SANISAND: simple anisotropic sand plasticity model."
443 *International Journal for Numerical and Analytical Methods in Geomechanics*, 32(8), 915-948.

444 Uchida, K., and Stedman, J. (2001). "Liquefaction behaviour of Toyoura sand under cyclic strain
445 controlled triaxial loading." *Proc., Proceedings of the Eleventh International Offshore and Polar*
446 *Engineering Conference*, Stavanger, Norway, 17-22.

447 Verdugo, R., and Ishihara, K. (1996). "The steady state of sandy soils." *Soils and foundations*, 36(2), 81-
448 91.

449 Vermeer, P.A. (1978). "A double hardening model for sand." *Geotechnique*, 28(4), 414–433.

450 Wan, R., and Pouragha, M. (2015). "Continuum representation of granular fabric and connectivity."
451 *Continuum Mechanics and Thermodynamics*, 27: 243-259.

452 Wu, W., Bauer, E., and Kolymbas, D. (1996). "Hypoplastic constitutive model with critical state for
453 granular materials." *Mechanics of materials*, 23(1), 45-69.

454 Yang, J., and Sze, H.Y. (2011). "Cyclic behaviour and resistance of saturated sand under non-
455 symmetrical loading conditions." *Geotechnique*, 61(1), 59–73.

456 Yao, Y., Sun, D., and Luo, T. (2004). "A critical state model for sands dependent on stress and density."
457 *International Journal for Numerical and Analytical Methods in Geomechanics*, 28(4), 323-337.

458 Yao, Y., Sun, D., and Matsuoka, H. (2008). "A unified constitutive model for both clay and sand with
459 hardening parameter independent on stress path." *Computers and Geotechnics*, 35(2), 210-222.

460 Yin, Z.-Y., Chang, C. S., and Hicher, P.-Y. (2010). "Micromechanical modelling for effect of inherent
461 anisotropy on cyclic behaviour of sand." *International Journal of Solids and Structures*, 47(14), 1933-
462 1951.

463 Yin, Z.-Y., Zhao, J., and Hicher, P.-Y. (2014). "A micromechanics-based model for sand-silt mixtures."
464 *International journal of solids and structures*, 51(6), 1350-1363.

465 Yin, Z.-Y., and Chang, C. S. (2013). "Stress–dilatancy behavior for sand under loading and unloading
466 conditions." *International Journal for Numerical and Analytical Methods in Geomechanics*, 37(8),

855-870.

Yoshimine, M., Ishihara, K., and Vargas, W. (1998). "Effects of principal stress direction and intermediate principal stress on undrained shear behavior of sand." *Soils and Foundations*, 38(3), 179-188.

Yu, H. (1998). "CASM: A unified state parameter model for clay and sand." *International Journal for Numerical and Analytical Methods in Geomechanics*, 22(8), 621-653.

Table

Table 1 Values of model parameters for Toyoura sand

G_0 /kPa	υ	n	ϕ_c /°	e_{c0}	λ	ξ	d
3000	0.3	0.67	31.2	0.937	0.022	0.71	2

Figure captions

Fig. 1. Stress ratio versus shear strain described by (a) an hyperbolic function, (b) an exponential function, and (c) a modified incremental form of the exponential function.

Fig. 2. Schematic plot of a typical drained triaxial test with the definition of the model parameters

Fig. 3. Simulated results of undrained triaxial tests: (a) stress-path under monotonic loading, (b) deviatoric stress-strain under monotonic loading, (c) stress-path under cyclic loading, (d) deviatoric stress-strain under cyclic loading.

Fig. 4. Simulated results of drained constant-*p'* tests: (a) deviatoric stress-strain under monotonic loading, (b) volumetric strain versus deviatoric strain under monotonic loading, (c) deviatoric stress-strain under cyclic loading, (d) volumetric strain versus deviatoric strain under cyclic loading.

Fig. 5. Simulated results of conventional drained triaxial tests: (a) deviatoric stress-strain under monotonic loading, (b) volumetric strain versus deviatoric strain under monotonic loading, (c) deviatoric stress-strain under cyclic loading, (d) volumetric strain versus deviatoric strain under cyclic loading.

Fig. 6. Simulated results of drained constant-*p'* tests with two different initial void ratios: (a) deviatoric stress-strain, and (b) volumetric strain versus deviatoric strain.

Fig. 7. Different curves of CSL described by the enhanced equation: (a) effect of ξ, (b) effect of λ, and (c) effect of the combined parameters for an almost straight line.

Fig. 8. Simulated results of (a)-(c) undrained triaxial tests with different initial void ratios, and (d)-(f) drained triaxial tests with different initial void ratios.

Fig. 9. Simulated results of undrained triaxial tests with different initial void ratios with the influence of a non-linear stress-dilatancy.

Fig. 10. Parameters determination from three undrained triaxial tests on Toyoura sand isotropically compressed at 1000 kPa with different initial densities: (a) CSL in the e-logp' plane, (b) stress paths and (c) deviatoric stress versus deviatoric strain.

Fig. 11. Comparison between experimental and numerical results of drained triaxial compression tests on Toyoura sand with different initial void ratios under confining stresses of 100 kPa and 500 kPa.

Fig. 12. Comparison between experimental and numerical results of undrained triaxial compression tests on Toyoura sand with different initial void ratios under confining stresses from 100 kPa to 3000 kPa.

Fig. 13. Comparison between experimental and numerical results of constant-*p'* drained cyclic tests on Toyoura sand: (a)-(c) loose specimen, and (d)-(f) dense specimen.

Fig. 14. Comparison between experimental and numerical results for drained cyclic triaxial tests on Toyoura sand.

Fig. 15. Comparison between the experimental and numerical results of undrained triaxial tests under cyclic loading on Toyoura sand with different initial void ratios.

Fig. 16. Numerical results for undrained cyclic triaxial tests on Toyoura sand with three different initial void ratios.

Fig. 17. Numerical results for undrained cyclic triaxial tests on Toyoura sand with (a-b) three different initial stress ratios and (c-d) three different static deviatoric stresses.

Figure 1

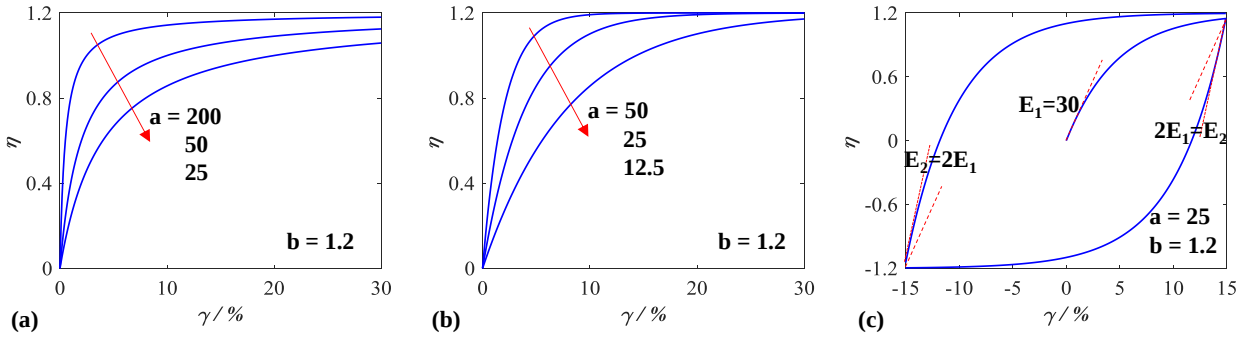
1.2
0.8
0.4
0
η
a = 200
50
25
b = 1.2
0
10
20
30
γ / %
(a)
1.2
0.8
0.4
0
η
a = 50
25
12.5
b = 1.2
0
10
20
30
γ / %
(b)
1.2
0.6
0
-0.6
-1.2
η
E1=30
2E1=E2
E2=2E1
a = 25
b = 1.2
-15
-10
-5
0
5
10
15
γ / %
(c)

Figure 2

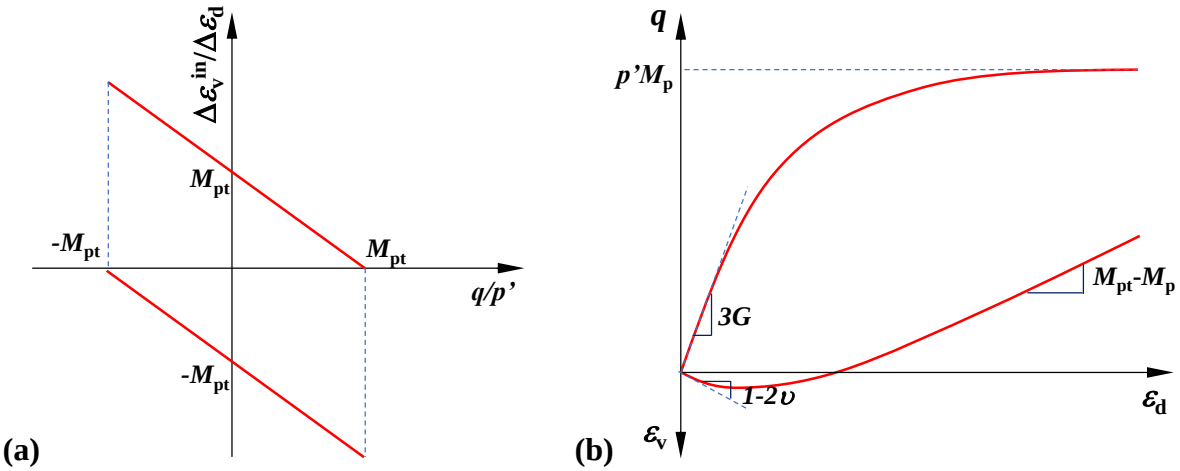
$\Delta\varepsilon_v^{in}/\Delta\varepsilon_d$
M_{pt}
$-M_{pt}$
M_{pt}
q/p'
$-M_{pt}$
(a)
q
$p'M_p$
$3G$
$1\text{-}2\upsilon$
$M_{pt}\text{-}M_p$
ε_d
ε_v
(b)

Figure 3.

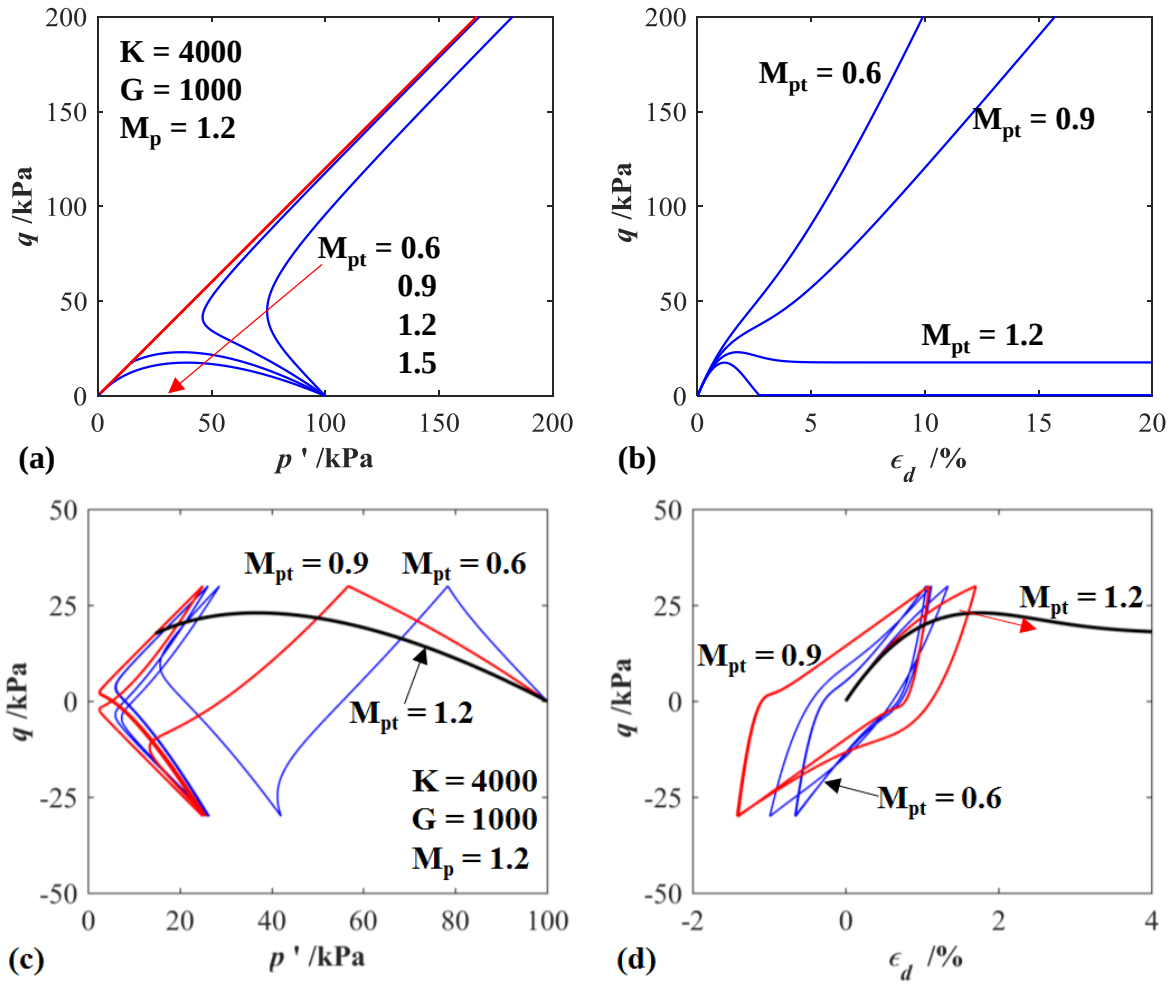

Figure 4.

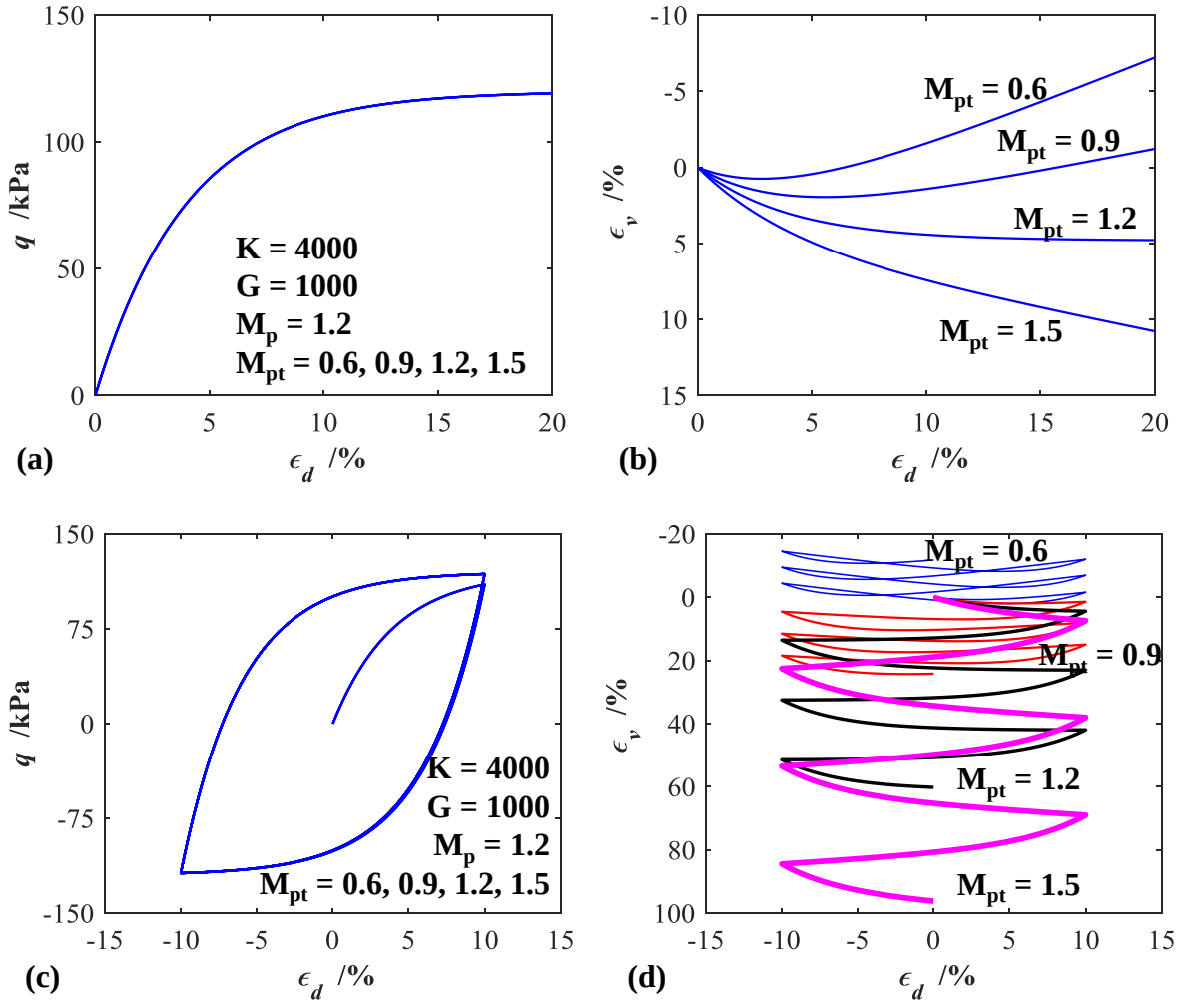

Figure 5.

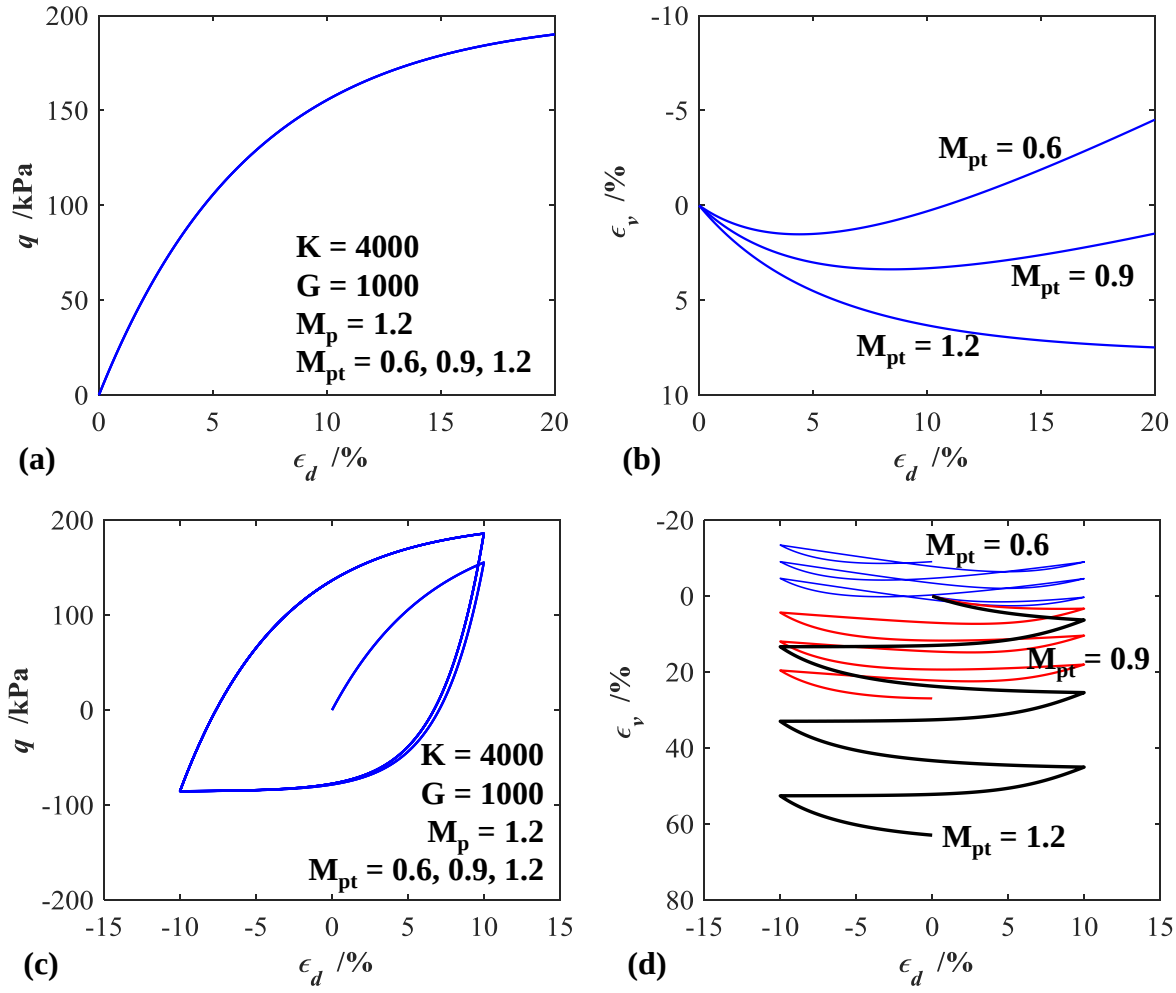

Figure 6.

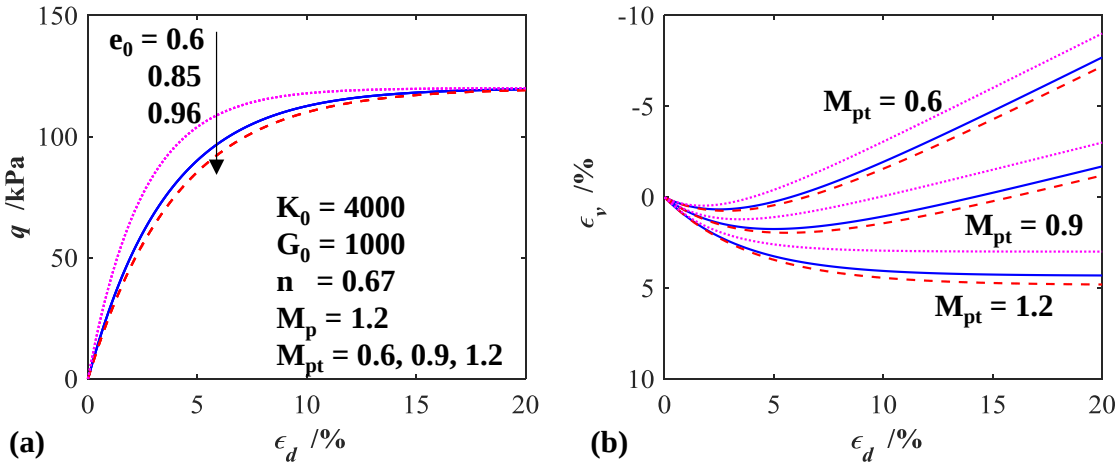

Figure 7.

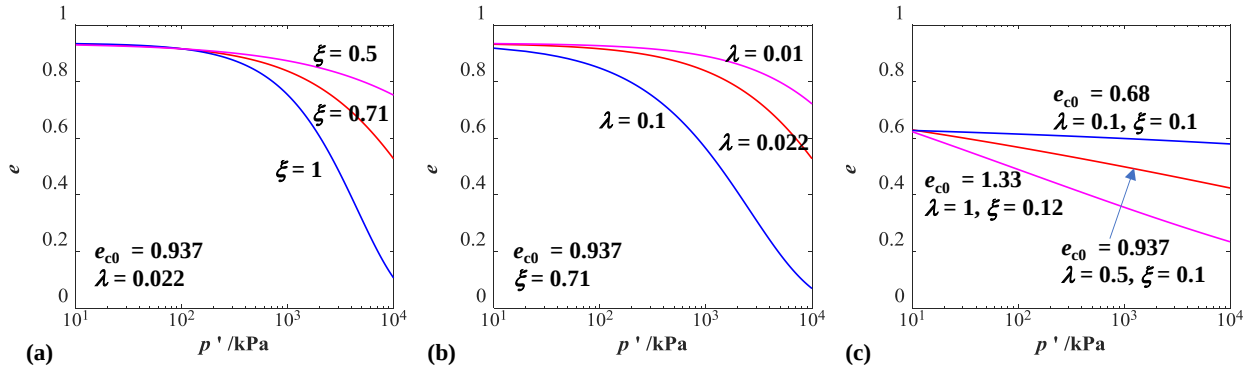

Figure 8.

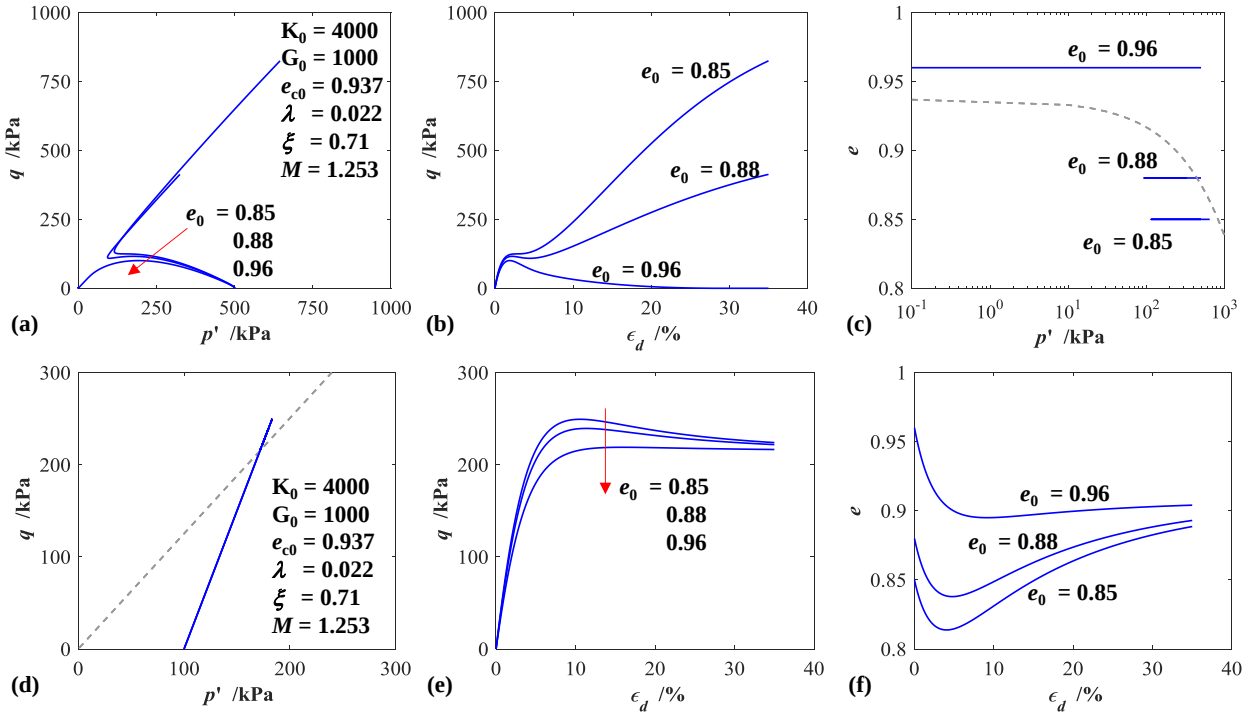

Figure 9.

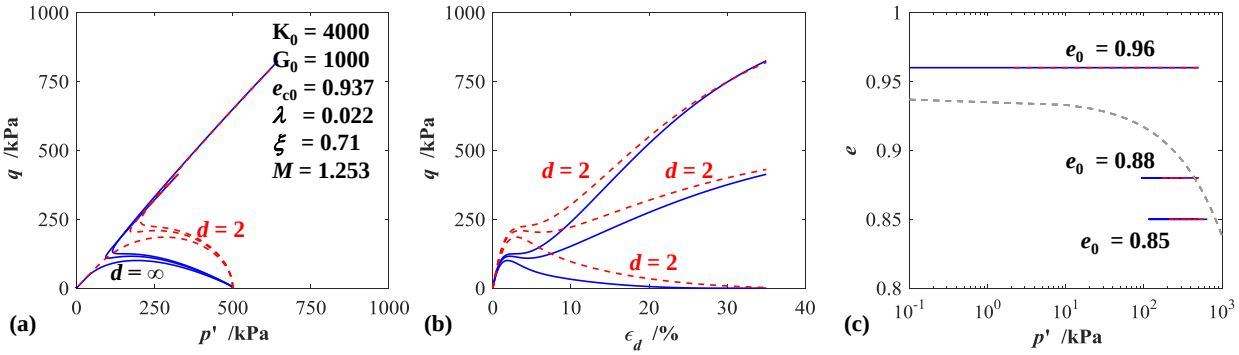

Figure 10.

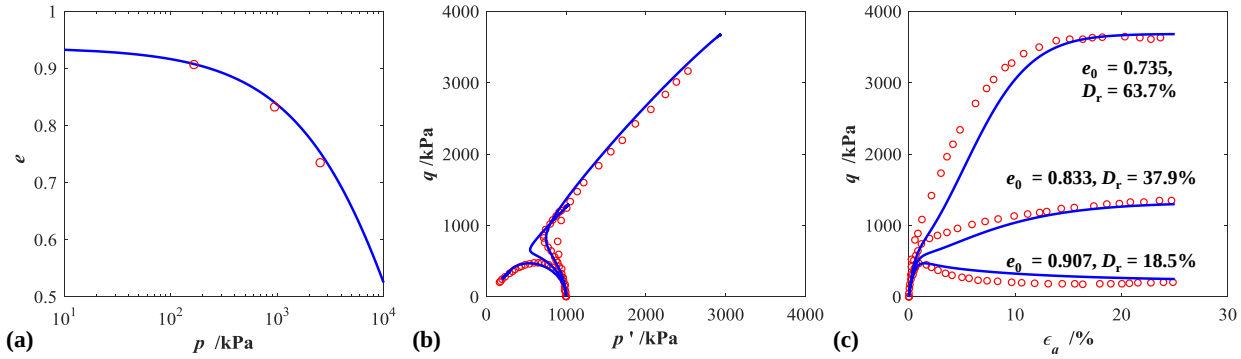

Figure 11

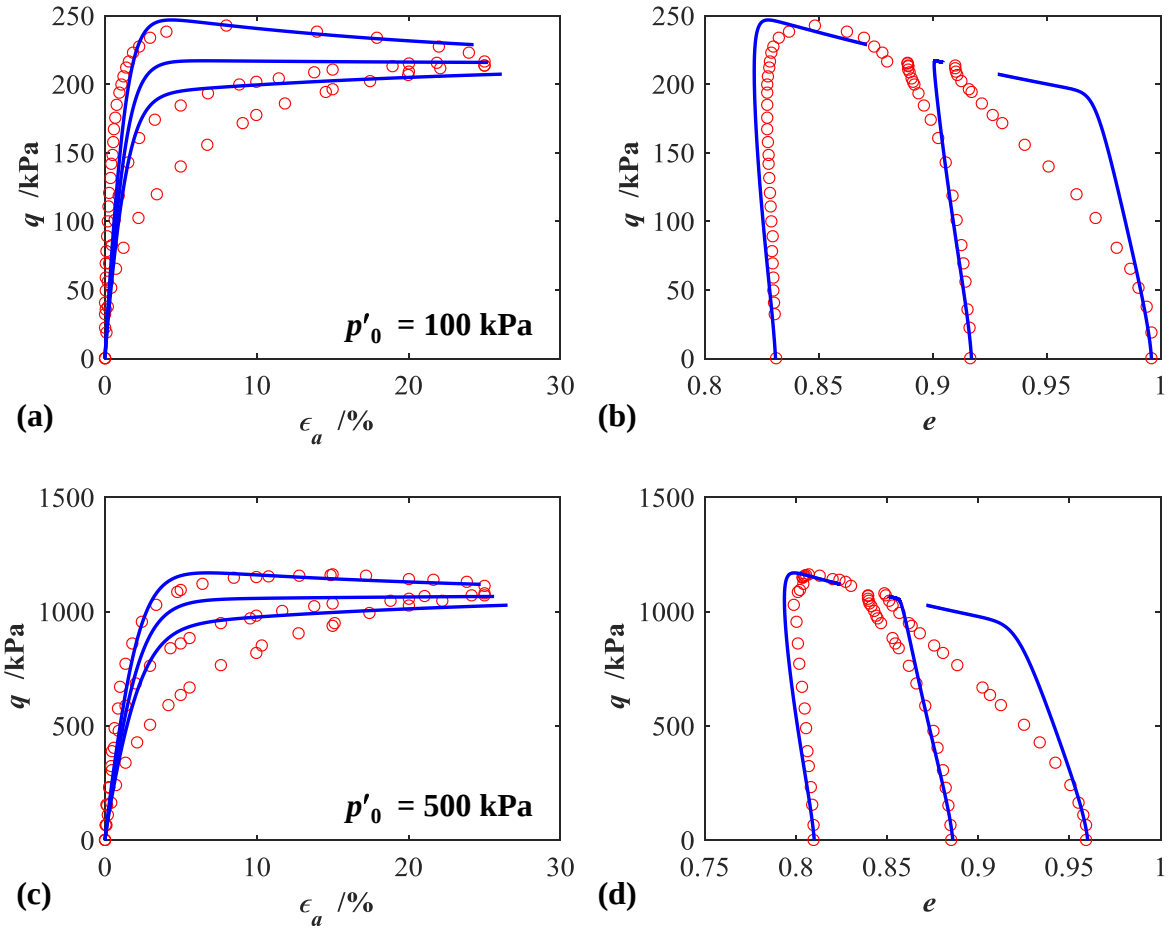

Figure 12

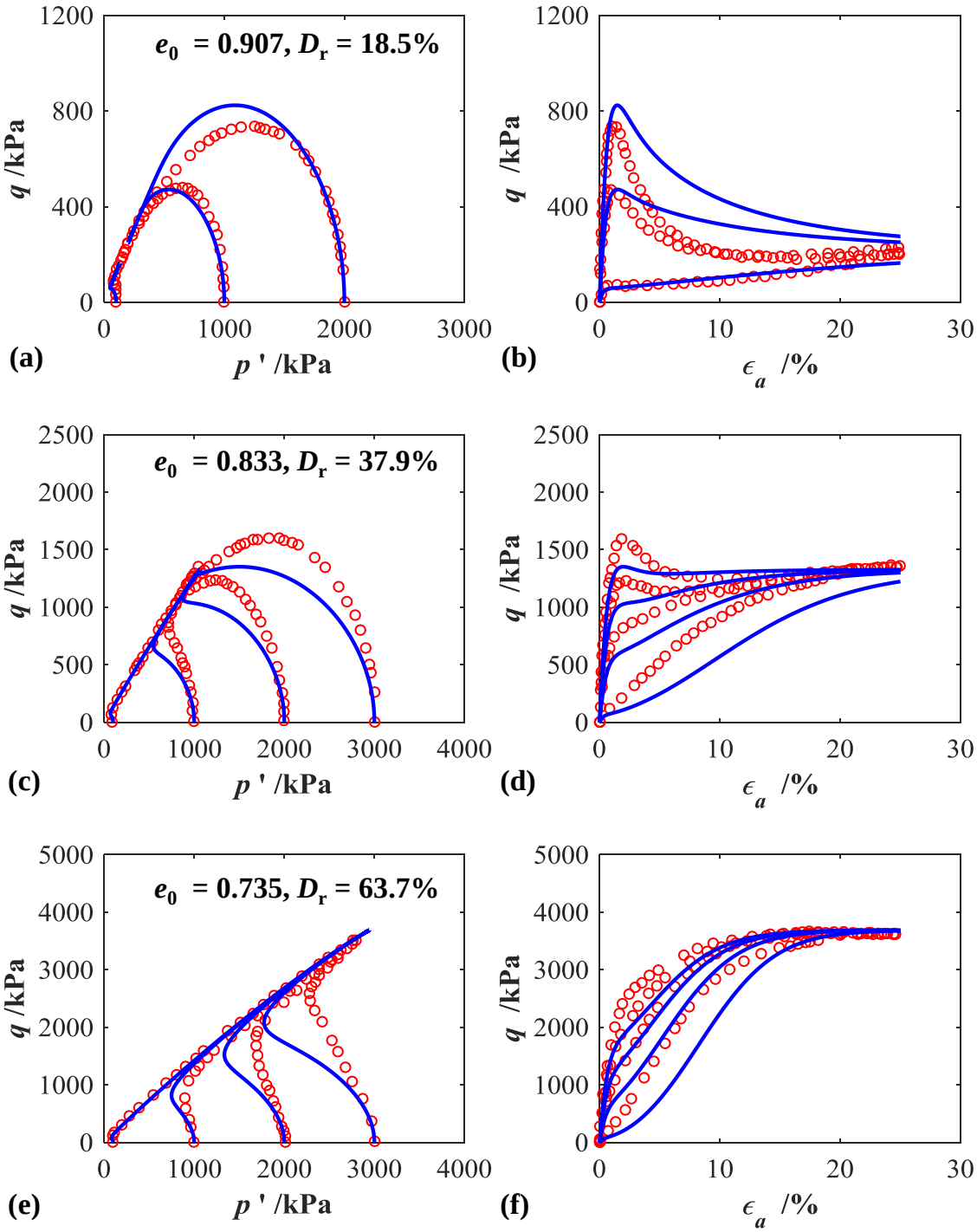

Figure 13

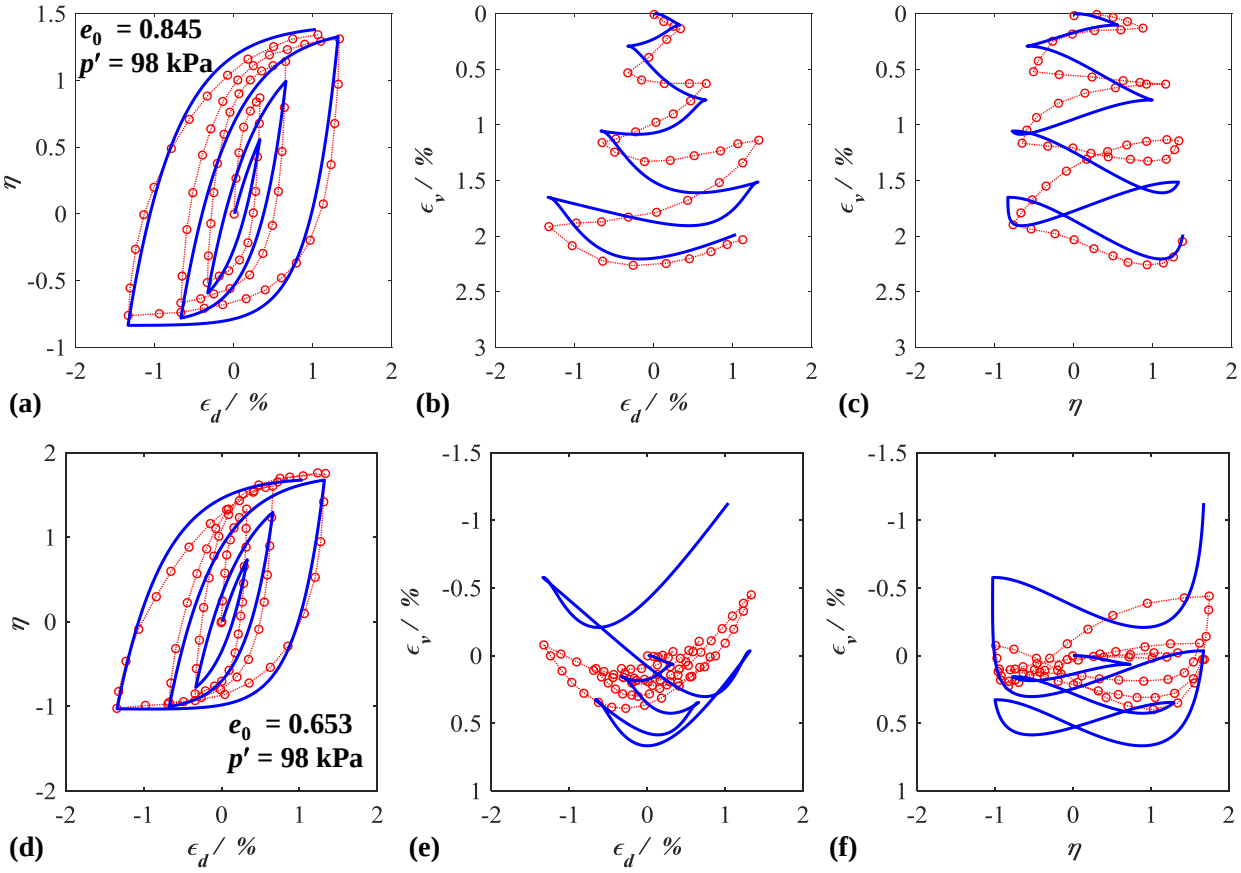

Figure 14

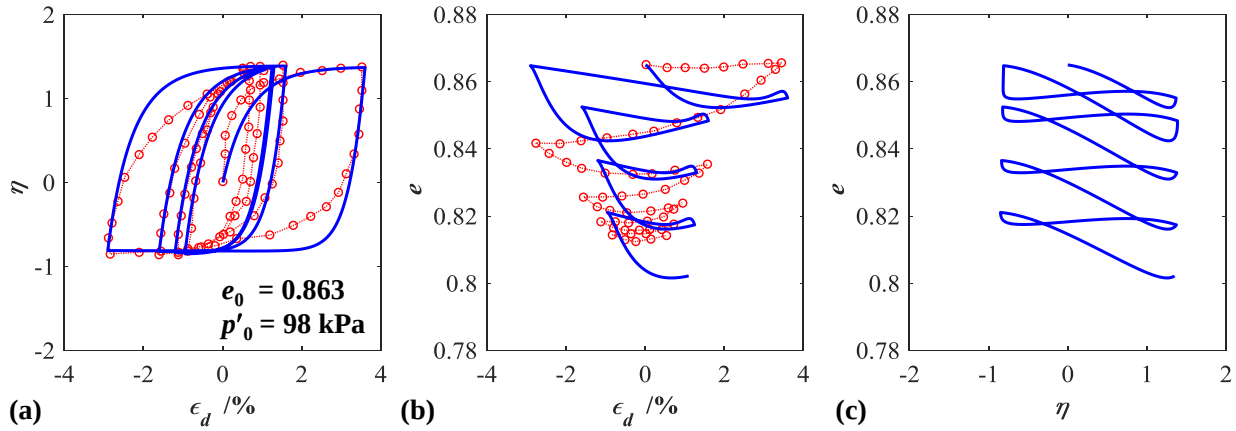

Figure 15

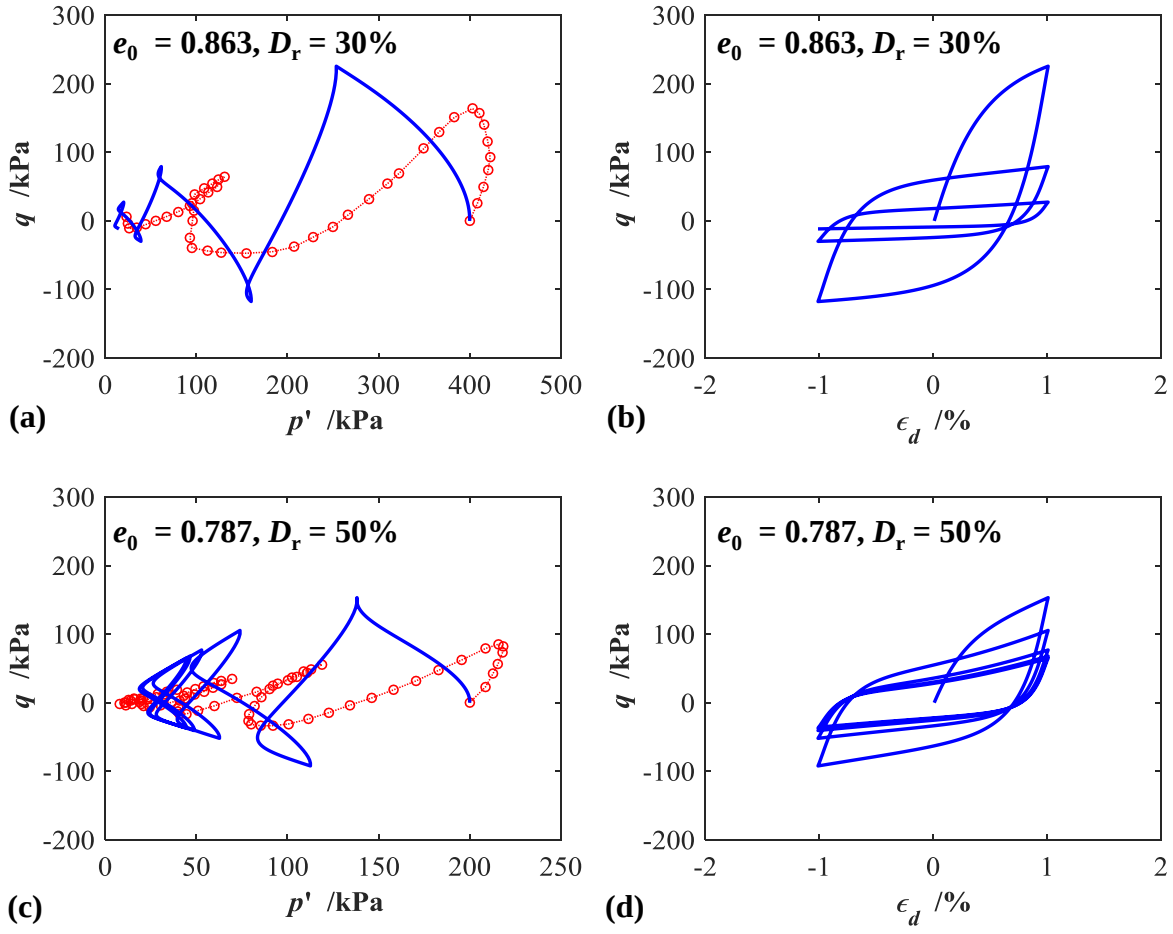
e0 = 0.863, Dr = 30%
q /kPa
p' /kPa
(a)
e0 = 0.863, Dr = 30%
q /kPa
ϵd /%
(b)
e0 = 0.787, Dr = 50%
q /kPa
p' /kPa
(c)
e0 = 0.787, Dr = 50%
q /kPa
ϵd /%
(d)

Figure 16

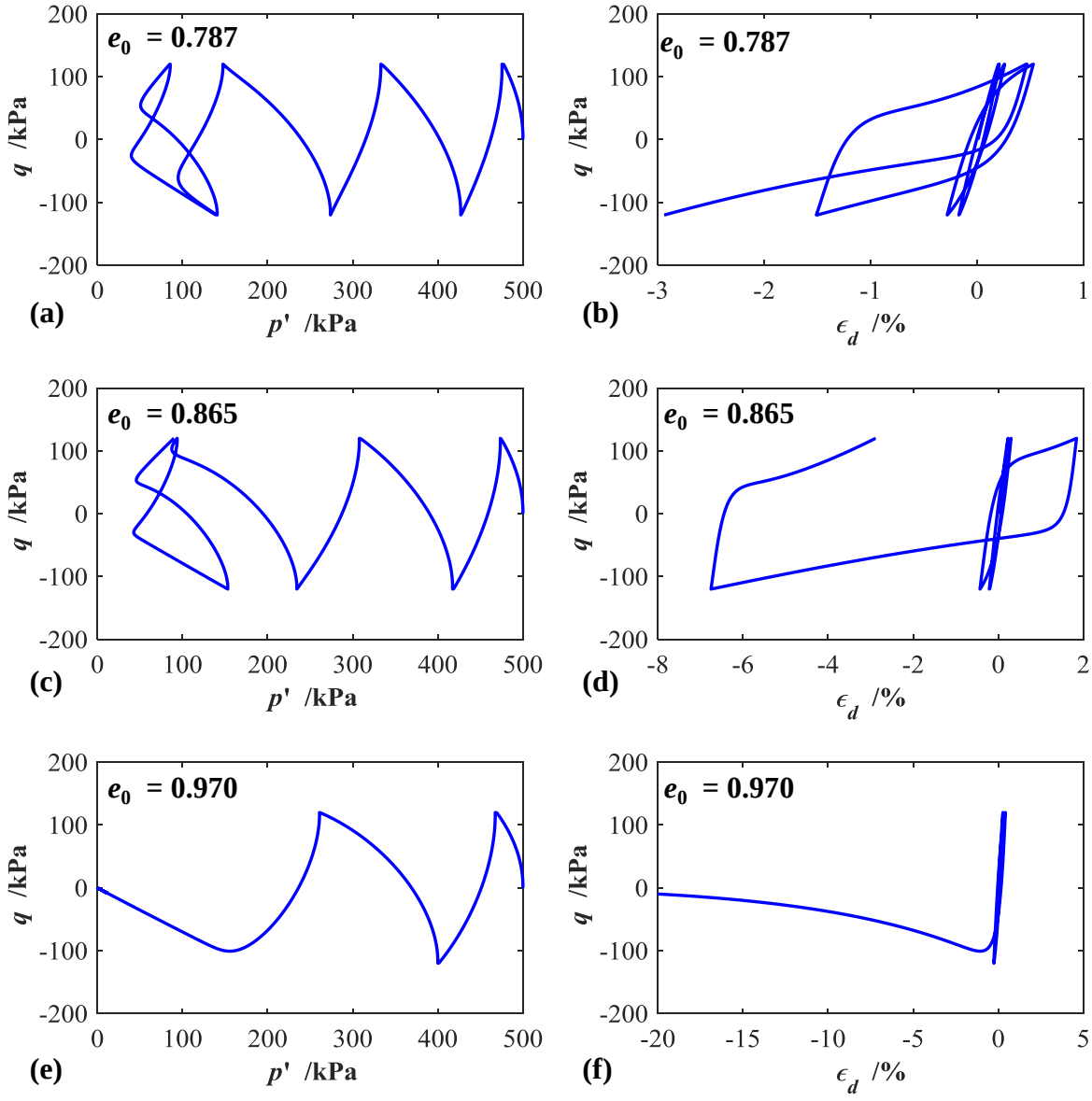

Figure 17